Observation of a Localized Flat-Band State in a Photonic Lieb Lattice

Sebabrata Mukherjee,[1,*] Alexander Spracklen,[1] Debaditya Choudhury,[1] Nathan Goldman,[2,3] Patrik Öhberg,[1] Erika Andersson,[1] and Robert R. Thomson[1]

[1]*SUPA, Institute of Photonics and Quantum Sciences, Heriot-Watt University, Edinburgh EH14 4AS, United Kingdom*
[2]*Center for Nonlinear Phenomena and Complex Systems, Université Libre de Bruxelles, CP 231, Campus Plaine,
B-1050 Brussels, Belgium*
[3]*Laboratoire Kastler Brossel, Collège de France, 11 Place Marcelin Berthelot, 75005 Paris, France*
(Received 22 December 2014; published 15 June 2015)

We demonstrate the first experimental realization of a dispersionless state, in a photonic Lieb lattice formed by an array of optical waveguides. This engineered lattice supports three energy bands, including a perfectly flat middle band with an infinite effective mass. We analyze, both experimentally and theoretically, the evolution of well-prepared flat-band states, and show their remarkable robustness, even in the presence of disorder. The realization of flat-band states in photonic lattices opens an exciting door towards quantum simulation of flat-band models in a highly controllable environment.

Introduction.—Transport in crystals reveals a rich variety of phenomena, ranging from dissipationless currents in superconductors to spin-polarized edge states in topological insulators. Importantly, both classical and quantum transport can show localization effects, which typically depend on the dimensionality, presence of disorder or impurities, and nature of interparticle interactions. Localization phenomena include disorder-induced (Anderson) localization, which is now well established in noninteracting systems [1], and also many-body localization, as recently explored in disordered cold atomic gases [2]. Interestingly, localization can also exist in lattices without disorder. Indeed, specific lattice geometries can allow for destructive wave interference, leading to perfectly flat (dispersionless) energy bands where particles exhibit infinite effective mass. Perhaps the simplest lattice where this phenomenon occurs is the two-dimensional Lieb lattice, Fig. 1(a), which belongs to a wide family of flat-band models [3–9]. Originally, flat-band Hubbard models were analyzed in the context of magnetism, where electrons populating the flat band were found to contribute to unusual ferromagnetic ground states [7]. More recently, the interplay between flat-band localization and correlated disorder was studied in Ref. [10].

It is intriguing that slight changes in the tunneling matrix elements between different lattice sites can lead to dramatically different transport properties, including exact localization associated with flat-band states. Different physical platforms, including cold atoms in optical lattices [11–13] and light propagation in photonic crystals [14,15], have been envisaged to reveal flat-band properties through the engineering of exotic specific lattice models. Both cold atoms and photonic crystals offer a high control over the lattice geometry, and allow for the addition of tunable disorder or interactions [16,17]. This suggests an exciting

route for the quantum simulation of interacting flat-band systems. Recently, Guzman-Silva *et al.* [15] have reported bulk and edge transport phenomena in a photonic Lieb lattice. However, to date, diffraction-free propagation of a flat-band state has not been observed. In this Letter, we present the first experimental observation of a stationary and localized flat-band state in a photonic Lieb lattice, where the lattice is formed by a two-dimensional array of optical waveguides, fabricated using femtosecond laser writing [18].

Light propagation in an array of evanescently coupled optical waveguides, i.e., a photonic lattice, is in the paraxial approximation described by a Schrödinger equation

$$i\partial_z \Psi(x,y,z) = \left[-\frac{1}{2k_0 n_0} \nabla_\perp^2 - k_0 \Delta n(x,y,z) \right] \Psi(x,y,z),$$

(1)

where the refractive index profile across the lattice $[\Delta n(x,y,z)]$ acts as an effective potential for the light field. The role of the wave function is played by the envelope of the electric field $E(x,y,z) = \Psi(x,y,z)e^{i(k_0 z - \omega t)}$, where k_0 is the free-space wave number and n_0 is the refractive index of the host material in which the lattice is created. By controlling the refractive index (Δn) profile across the lattice structure, one may use photonic lattices to observe and probe phenomena from solid-state physics, such as Bloch oscillations [19–22], dynamic localization [23], Bloch-Zener oscillations [24], and Landau-Zener tunneling [25].

For weak evanescent coupling, Eq. (1) can be modeled by a tight-binding Hamiltonian. In this Letter we consider an edge-centered square (Lieb) lattice, as shown in Fig. 1(a). By Fourier transforming the Hamiltonian into k space, we obtain an energy spectrum with three bands,
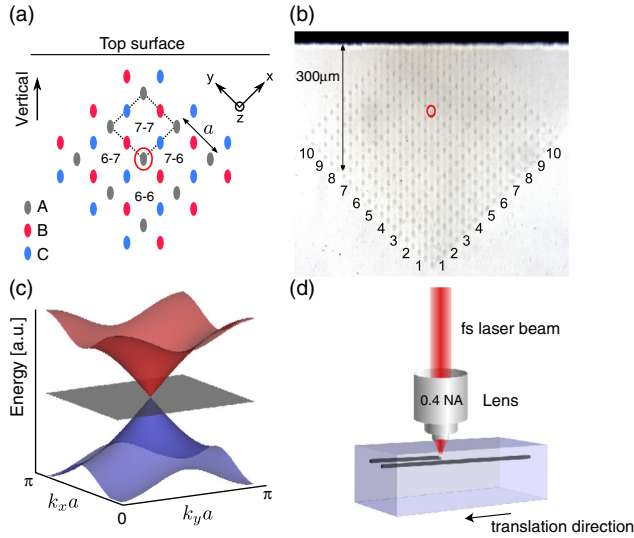
FIG. 1 (color online). (a) Edge-centered square (Lieb) lattice. The basis contains three sites (A, B, and C). To avoid edge effects and effects due to lattice inhomogeneity with depth, all measurements were performed near the circled A site (A_{7-7}); see also (b). The lattice constant $a = 44$ μm. (b) White-light transmission optical micrograph of the facet of a Lieb lattice with 323 waveguides fabricated by femtosecond laser writing. Each waveguide supports only a single fundamental mode at 780 nm. The next-nearest-neighbor coupling for a 7-cm-long glass chip was observed to be negligible. To minimize the difference in the next-nearest-neighbor coupling constants along the x and y axes, the lattice was fabricated such that the x and y axes of the lattice were at 45° relative to the vertical axis. (c) Representation of the three energy bands, including the flat band in the middle, for $\{k_x a, k_y a\} = [0, \pi]$. (d) The femtosecond laser-writing technique.

$$\Omega_{\pm}(\mathbf{k}) = \pm 2\sqrt{\kappa_x^2 \cos^2(k_x a) + \kappa_y^2 \cos^2(k_y a)}, \quad (2)$$

$$\Omega_0(\mathbf{k}) = 0, \quad (3)$$

where κ_x and κ_y are the hopping amplitudes (coupling constants) for nearest-neighbor sites along the x and y axes, and a is the lattice constant. $\Omega_{\pm}$ are the energies of the upper and the lower bands, respectively, and Ω_0 represents the nondispersive flat band. The Brillouin zone spans $0 < k_x, k_y < \pi/a$. The three bands intersect at $k_x = k_y = \pi/2a$, known as the M point, see Fig. 1(c).

The lattice Hamiltonian displays particle-hole symmetry. This symmetry, combined with the statement that at each $\mathbf{k}$ there are three energy states, automatically implies a flat band; as for each $\mathbf{k}$, one of these energies must be zero. This argument breaks down in presence of disorder, as $k_{x,y}$ are no longer good quantum numbers. However, as shown in the Supplemental Material [26], the flat band persists for off-diagonal disorder (i.e., disordered coupling constants) of arbitrary strength. This form of disorder is present in our lattices, and is due to small random variations in

waveguide-to-waveguide separations across and along the lattice. In contrast, diagonal disorder would occur if different waveguides exhibited random variations in their propagation constants. As we discuss later, this form of disorder is not significant in our lattices.

The dotted square in Fig. 1(a) shows a primitive cell of the lattice. There are four A sites at the corners of each cell: two B sites and two C sites lie on the edges. If the Lieb lattice is isotropic, with $\kappa_x = \kappa_y$, then a superposition of states in the flat band can be excited if (a) the lattice has insignificant next-nearest-neighbor coupling, and (b) the two B sites and two C sites of a primitive cell are excited with equal intensities ($I_B = I_C$) and alternating phases ($\phi_B = \phi_C \pm \pi$). In this Letter, we demonstrate experimentally and theoretically that the flat-band state excited at the input of a photonic Lieb lattice remains localized and does not diffract.

Fabrication of photonic Lieb lattice.—Photonic Lieb lattices were fabricated using femtosecond laser writing, a well-established laser fabrication technique [18]. The substrate material (Corning Eagle^{2000}) was mounted on air-bearing Aerotech $x - y - z$ translation stages (ABL1000), and each lattice waveguide was fabricated by translating the substrate once through the focus of a 500-kHz train of circularly polarized subpicosecond ($\sim$400 fs) laser pulses, generated by a Menlo BlueCut fiber laser system. The laser-writing parameters were optimized to produce low propagation loss, single-mode waveguides for operation at a wavelength of 780 nm. The waveguide refractive index profile was controlled using the slit-beam shaping method [27,28], by placing a slit directly in front of the 0.4 numerical aperture (NA) lens used to focus the laser pulses inside the substrate. The effective NAs of the laser focus were calculated to be $\approx$0.2 and 0.3, along the axis perpendicular and parallel to the waveguide axis, respectively. The final Lieb lattices were inscribed in a 7-cm-long glass chip. Individual waveguides exhibited propagation loss of $\approx$1 dB/cm at 780 nm.

Thirteen complete Lieb lattices (lattice constant $a = 24$–48 μm in steps of 2 μm) were fabricated, each containing 323 single-mode waveguides. However, as discussed later, it was not possible to observe the non-diffracting state when $a \leq 42$ μm, because next-nearest-neighbor coupling in these lattices is non-negligible over the 7-cm length of the chip, destroying the flat band. The remainder of the Letter shall, therefore, focus on the lattice fabricated with $a = 44$ μm, the most compact Lieb lattice fabricated where the flat band could be excited. A white-light transmission optical micrograph of the facet of this lattice is shown in Fig. 1(b). The individual waveguide modes are slightly elliptical in shape, supporting a single mode at 780 nm with major and minor mode-field diameters of 8.6 and 7.4 μm along the vertical and horizontal axis, respectively. To minimize differences in nearest-neighbor coupling coefficients along the x and y

axes, the lattice was fabricated such that the x and y axes were at 45° relative to the vertical and horizontal axis, Fig. 1(b).

Optical characterization and excitation of photonic Lieb lattice.—It is well known that for femtosecond laser writing, depth-dependent aberrations imparted on the laser beam by the air-glass interface can significantly affect the properties of the written waveguides [29]. This will clearly result in depth-dependent lattice properties. To assess the homogeneity of the fabricated Lieb lattice, we investigated how the coupling constant between two evanescently coupled waveguides varied as a function of depth. We inscribed arrays of two-waveguide evanescent field couplers at six different depths, from 100 to 600 μm in steps of 100 μm. Each coupler was fabricated using the same waveguide-to-waveguide separation in the interaction region (22 μm), and same waveguide-to-waveguide angle [relative to the vertical axis in Fig. 1(a)] as the waveguides in the Lieb lattice. At each depth, five sets of 17 couplers were fabricated, each set consisting of couplers with interaction lengths between 1 and 65 mm, in steps of 4 mm. Each coupler was characterized by injecting 780-nm light into one of the waveguides and measuring the output coupling ratio. Using this data, and the procedure outlined in [30], the mean and standard deviation of the coupling constant at each depth was evaluated to be ≈ 0.01 mm^{-1} and ≈ 0.002 mm^{-1}, respectively, for couplers fabricated up to a maximum depth of 300 μm. After this, both the coupling constant and variance were observed to become a function of depth, with deeper structures exhibiting a progressively higher variance.

To investigate whether the observed variation in coupling constant was due to random variations in the waveguide-to-waveguide separation (off-diagonal disorder), or random variations in waveguide propagation constants (diagonal disorder), we performed a second set of experiments, where an array of couplers with different interaction lengths were fabricated at a single depth inside the substrate. The waveguide-to-waveguide angle and separation in the interaction region were set to 45° and 15 μm, respectively; the reduced interaction separation was used to reduce the coupling length. Coupling characteristics for these couplers were observed to be close to ideal, with near-complete transfer of power from the input waveguide to the other waveguide achieved after one coupling length. Since complete transfer of energy from one waveguide to another in an evanescent field coupler is only possible if the waveguides support modes with identical propagation constants, we conclude that local variations in waveguide propagation constants are negligible in our Lieb lattices. Hence, diagonal disorder is not significant.

Given the results outlined above, all optical measurements of the Lieb lattice were performed by injecting light into the primitive sites surrounding the A_{7-7} site [circled in Fig. 1(b)], which is at a depth of ≈ 150 μm. First, 780-nm

light was individually coupled to the nine A, six B, and six C sites surrounding the A_{7-7} site, and the output diffraction patterns were measured. For each type of injection site, the obtained diffraction patterns were normalized and averaged. The results of these measurements are presented in Fig. 2, where the sites excited at the input are circled. It can clearly be seen that the circled A site in Fig. 2(a) contains less light than the circled B site in Fig. 2(b), or the circled C site in Fig. 2(c), confirming that light injected into A sites diffracts more than light injected into B or C sites. This has been recently shown by Guzman-Silva *et al.* [15].

Figure 3(a) shows a schematic of the experimental setup used to excite the flat-band state. Laser light of 780 nm emerging from a single-mode fiber was collimated using lens L_1. This light was then focused through a zero-order nulled (for 780 nm) DOE (binary-phase, square-checkerboard pattern) using lens L_2, to generated a square array of diffracted orders at the focus of L_2. Using lenses L_3 and L_4, these diffraction orders were relay imaged to the spatial filter, which blocks all orders, except for the four first-order spots. Using lenses L_5 and L_6, the four spots were relay imaged to the input facet of the Lieb lattice [Fig. 3(b)]. The size of each spot on the lattice facet could be controlled via the diameter of the beam entering lens L_6 and its focal length, and the spacing between the spots could be controlled via the distance of the DOE from lens L_2. The relative optical phases between the spots could be inferred by viewing the four-spot interference pattern in the Fraunhofer regime (using a camera not shown). As shown in Figs. 3(c) and 3(d), the relative phases between the spots could be controlled by translating the DOE in the $x - y$ plane (the z axis is the beam propagation axis). Independent control over the spacing and size of the four spots on the facet of the Lieb lattice enabled simultaneous excitation of two B-site and two C-site waveguides for a given primitive cell. To couple the spots to the lattice in a controllable manner, 780 ± 10-nm light from a filtered broadband source was used to flood illuminate the output end of the lattice and excite all the guided modes. Using camera 1, it was thus possible to simultaneously view both the lattice
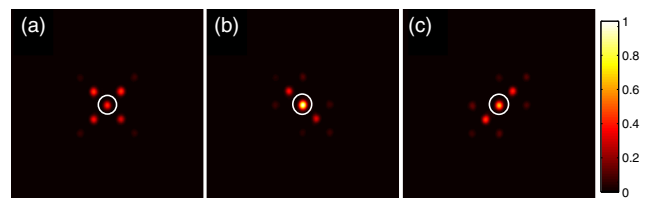

FIG. 2 (color online). Average diffraction patterns when (a) A, (b) B, and (c) C sites surrounding A_{7-7} were excited separately. The excited sites are circled. Each image is normalized such that the total output power is 1, and the field of view is approximately 225 μm $\times$ 225 μm. Simulations based on these averaged diffraction patterns indicate a waveguide-to-waveguide coupling constant of 0.01 ± 0.001 mm^{-1}.
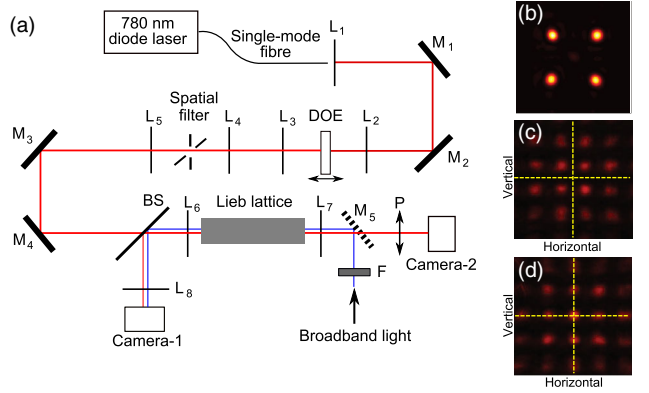
FIG. 3 (color online). (a) Experimental setup for exciting the flat band. L_1–L_8 are convex lenses, M_1–M_5 are silver-coated mirrors with M_5 on a flipped mount, and BS is a beam splitter. L_1 collimated the 780-nm light emerging from a single-mode fiber. A zero-order nulled, binary-phase, square-checker-board diffractive optical element (DOE) generated a square array of diffraction-order "spots" at the focus of L_2. Using L_3 and L_4, these spots were relay imaged to the spatial filter, the transmission aperture of which was adjusted to pass only the four first orders (and a very weak 0th order). Using L_5 and L_6, the four spots were relay imaged to the input facet of the Lieb lattice. The output facet of the lattice was flood illuminated using 780 ± 10-nm light, filtered from a broadband white-light source using a bandpass filter (F). This flood illumination excited the lattice modes, and enabled precise alignment of the four spots with the desired waveguide modes using camera 1. Once light had been coupled to the lattice, the light distribution at the output facet could be viewed using camera 2. A polarizer (P) passing only vertically polarized light was placed in front of camera 2, ensuring that measurements were not affected by polarization-dependent coupling in the lattice. (b) Intensity profile of the four spots that were coupled into the lattice (field of view approximately 80 μm × 80 μm). Note the very weak 0th order. (c)–(d) Fraunhofer diffraction patterns for the flat-band state and equal-phase state, respectively. The yellow dotted lines represent the positions of the optic axis.

modes and the excitation spots, enabling us to launch light specifically to the modes of the lattice.

To excite the flat-band state, the DOE position was set to produce four equal-intensity spots [relative standard deviation (RSD): 5.7%], with alternating 0 and π phases, Fig. 3(c). These four spots were then coupled to the B and C sites for the chosen primitive cell. A proof that such a state will excite the flat band is given in the Supplemental Material [26]. The (7–7), (6–7), (7–6), and (6–6) primitive cells were each excited, and the output diffraction patterns observed using camera 2. As shown in Figs. 4(a)–4(d), when the flat-band state was excited, no significant tunneling of light into the surrounding lattice sites could be observed after 7 cm of propagation. Nondiffracting states remain localized. Absence of diffraction was not observed in lattices with $a \leq 42$ μm, which we attribute to non-negligible next-nearest-neighbor coupling.
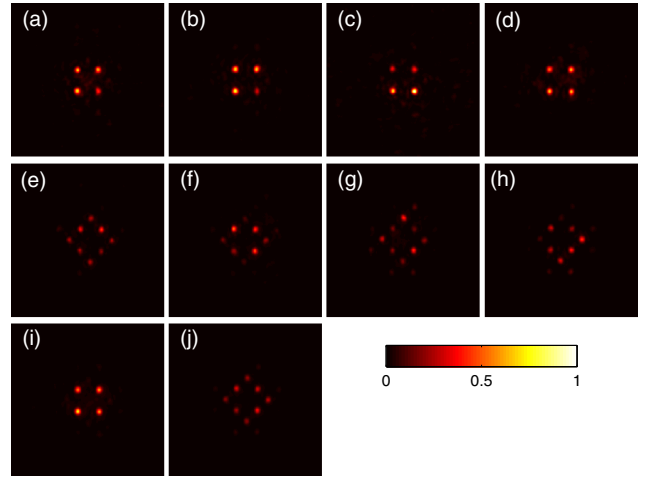

FIG. 4 (color online). (a)–(d) The nondiffracting states observed at the output of the lattice when the flat-band state was launched into the B and C sites of the (7–7), (6–7), (7–6), and (6–6) cells, respectively. When the equal-phase state was launched into the same cells, the output state is not localized, as shown by (e)–(h). (i) The average diffraction pattern of (a)–(d) and (j) is the average diffraction pattern of (e)–(h). Each image is normalized so that total intensity is 1. The field of view is approximately 210 μm × 210 μm.

To confirm that the observed absence of diffraction is particular to the phase and intensity distribution of the injected state, we coupled another state to the lattice, where B and C sites of a primitive cell are excited with close to equal intensity (RSD: 5.7%) but equal phase (the equal-phase state), Fig. 3(d). As presented in Figs. 4(e)–4(h), this state is not localized when injected into the (7–7), (6–7), (7–6), and (6–6) primitive cells, due to its orthogonality to the flat-band state. Interestingly, the diffraction patterns shown in Figs. 4(e)–4(h) are different, depending on which cell is excited, due to off-diagonal disorder. As discussed earlier, we are still able to successfully excite the flat band (see also Supplemental Material [26] for a theoretical description).

Conclusions.—We have experimentally excited a flat-band state in a photonic Lieb lattice, and observed nondiffractive propagation. Such states may provide useful applications in, for instance, image processing and precision measurements. It would be intriguing to extend this study to the case where nonlinearities are present. This would provide a platform to simulate and investigate the behavior of interacting particles with flat dispersion relations, suggesting an interesting route towards strongly correlated states of matter in photonic systems [31,32].

Note added.—We recently became aware of similar work by Vicencio *et al.* [33].

---

*snm32@hw.ac.uk

[1] J. Billy, V. Josse, Z. Zuo, A. Bernard, B. Hambrecht, P. Lugan, D. Clément, L. Sanchez-Palencia, P. Bouyer, and A. Aspect, Nature (London) **453,** 891 (2008).

[2] M. Schreiber, S. S. Hodgman, P. Bordia, H. P. Lüschen, M. H. Fischer, R. Vosk, E. Altman, U. Schneider, and I. Bloch, arXiv:1501.05661.

[3] A. Mielke, J. Phys. A **25,** 4335 (1992).

[4] H. Aoki, M. Ando, and H. Matsumura, Phys. Rev. B **54,** R17296(R) (1996).

[5] S. Deng, A. Simon, and J. Köhler, J. Solid State Chem. **176,** 412 (2003).

[6] C. Wu, D. Bergman, L. Balents, and S. Das Sarma, Phys. Rev. Lett. **99,** 070401 (2007).

[7] H. Tasaki, Eur. Phys. J. B **64,** 365 (2008).

[8] Z. Lan, N. Goldman, and P. Öhberg, Phys. Rev. B **85,** 155451 (2012).

[9] T. Jacqmin, I. Carusotto, I. Sagnes, M. Abbarchi, D. D. Solnyshkov, G. Malpuech, E. Galopin, A. Lemaître, J. Bloch, and A. Amo, Phys. Rev. Lett. **112,** 116402 (2014).

[10] J. D. Bodyfelt, D. Leykam, C. Danieli, X. Yu, and S. Flach, Phys. Rev. Lett. **113,** 236403 (2014).

[11] R. Shen, L. B. Shao, B. Wang, and D. Y. Xing, Phys. Rev. B **81,** 041410 (2010).

[12] V. Apaja, M. Hyrkäs, and M. Manninen, Phys. Rev. A **82,** 041402 (2010).

[13] N. Goldman, D. F. Urban, and D. Bercioux, Phys. Rev. A **83,** 063601 (2011).

[14] R. A. Vicencio and C. Mejía-Cortés, J. Opt. **16,** 015706 (2014).

[15] D. Guzmán-Silva, C. Mejía-Cortés, M. A. Bandres, M. C. Rechtsman, S. Weimann, S. Nolte, M. Segev, A. Szameit, and R. A. Vicencio, New J. Phys. **16,** 063061 (2014).

[16] I. Bloch, J. Dalibard, and W. Zwerger, Rev. Mod. Phys. **80,** 885 (2008).

[17] I. Carusotto and C. Ciuti, Rev. Mod. Phys. **85,** 299 (2013).

[18] K. M. Davis, K. Miura, N. Sugimoto, and K. Hirao, Opt. Lett. **21,** 1729 (1996).

[19] T. Pertsch, P. Dannberg, W. Elflein, A. Bräuer, and F. Lederer, Phys. Rev. Lett. **83,** 4752 (1999).

[20] R. Morandotti, U. Peschel, J. S. Aitchison, H. S. Eisenberg, and Y. Silberberg, Phys. Rev. Lett. **83,** 4756 (1999).

[21] G. Lenz, I. Talanina, and C. M. de Sterke, Phys. Rev. Lett. **83,** 963 (1999).

[22] N. Chiodo, G. D. Valle, R. Osellame, S. Longhi, G. Cerullo, R. Ramponi, P. Laporta, and U. Morgner, Opt. Lett. **31,** 1651 (2006).

[23] F. Dreisow, M. Heinrich, A. Szameit, S. Doering, S. Nolte, A. Tuennermann, S. Fahr, and F. Lederer, Opt. Express **16,** 3474 (2008).

[24] F. Dreisow, A. Szameit, M. Heinrich, T. Pertsch, S. Nolte, A. Tünnermann, and S. Longhi, Phys. Rev. Lett. **102,** 076802 (2009).

[25] F. Dreisow, A. Szameit, M. Heinrich, S. Nolte, A. Tünnermann, M. Ornigotti, and S. Longhi, Phys. Rev. A **79,** 055802 (2009).

[26] See Supplemental Material at http://link.aps.org/supplemental/10.1103/PhysRevLett.114.245504 for a more detailed description of the input flat-band state and the role of disorder in the lattice.

[27] M. Ams, G. Marshall, D. Spence, and M. Withford, Opt. Express **13,** 5676 (2005).

[28] Y. Cheng, K. Sugioka, K. Midorikawa, M. Masuda, K. Toyoda, M. Kawachi, and K. Shihoyama, Opt. Lett. **28,** 55 (2003).

[29] P. S. Salter, M. Baum, I. Alexeev, M. Schmidt, and M. J. Booth, Opt. Express **22,** 17644 (2014).

[30] S. M. Eaton, W.-J. Chen, H. Zhang, R. Iyer, J. Li, M. Ng, S. Ho, J. Aitchison, and P. R. Herman, J. Lightwave Technol. **27,** 1079 (2009).

[31] R. O. Umucalilar and I. Carusotto, Phys. Rev. Lett. **108,** 206809 (2012).

[32] M. F. Maghrebi, N. Y. Yao, M. Hafezi, T. Pohl, O. Firstenberg, and A. V. Gorshkov, Phys. Rev. A **91,** 033838 (2015).

[33] R. A. Vicencio, C. Cantillano, L. Morales-Inostroza, B. Real, C. Mejía-Cortés, S. Weimann, A. Szameit, and M. I. Molina, Phys. Rev. Lett. **114,** 245503 (2015).